PNAS
www.pnas.org

Supplementary information for

# Highly motile nanoscale magnetic artificial cilia

Tanveer ul Islam, Yves Bellouard, Jaap M J den Toonder*

Correspondence to; E-mail: J.M.J.d.Toonder@tue.nl.

**This PDF file includes:**

Supplementary Text S1 and S2
Figs. S1 to S6
Tables S1
Captions for Movies S1 to S12
References 1 to 7

**Other Supplementary Materials for this manuscript include the following:**

Movies S1 to S12

## Supplementary Text

S1. Molding process

The molding process uses commercially available PCTE membranes (it4ip-Belgium) as templates for shaping the magnetic fluid into cilia structures of different diameters and lengths.

Schematically shown in Fig. S1, the process starts with selecting a glass substrate to build the device on. A 200 $\mu m$ thick layer of PDMS is spin coated at 300 $rpm$ for 60 seconds on the substrate and heat cured in a $65^0C$ oven for a couple of hours. Using the edge of a glass slide or a round 3 $mm$ glass rod, the prepared magnetic fluid is pasted on the cured PDMS layer while maintaining a uniform thickness of less than a micrometer (Fig. S1A). All the cilia structures fabricated in this study are made from a fluid containing 40±2 $wt\%$ of magnetic particles. A thin ferrofluid layer on the PDMS membrane is preferred for better visualization of the cilia structures submerged in a fluid medium when viewed under a microscope using transmitted light mode (bottom illumination). PCTE molds are next pasted separately with a layer of ferrofluid filling the mold pores and then placed on the thin ferrofluid layer already pasted on the PDMS (Fig. S1B). The top face is topped up with extra ferrofluid to increase its thickness (Fig. S1C). PCTE mold with thickness less than 10 $\mu m$ are placed with smooth face facing down as the other face has a rough texture which is a consequence of the PCTE mold preparation process. The device is now held between two permanent magnets and put in a vacuum oven programmed to raise the temperature to $130^0C$ in about half an hour followed by 2 $hr$ delay and then ramp down to below $80^0C$ in the next half an hour (Fig. S1D). Removal of the cured device at a lower temperature of $80^0C$ is required to avoid the oxidation of the magnetite particles. Cilia fabricated by curing the magnetic fluid without the use of external magnets are found to show reduced response during actuation as the external magnets induce anisotropic magnetic response. The magnets induce a magnetic field of $0.15 - 0.2\,T$ directed along the cilia length. After curing, the washing process discussed further removes the heat modified PCTE mold.

The PCTE mold surrounded by the magnetic layers is peeled off from the PDMS membrane and plasma bonded to another 200 $\mu m$ thick PDMS layer, by activating both the surfaces using a plasma torch, to prevent detachment while washing (Fig. S1, E and F). Without bonding, the layers are held together by the weak adhesion force only which is mostly enough to hold layers together permanently. The device layers are now lifted from the glass substrate using a flat edged blade wetted in ethanol to reduce friction and avoid stretching of the layers (Fig. S1G). The lifted layers are immersed in a chloroform bath (10 $ml$) maintained in a petri-dishes and stirred for 5 minutes. Immersion in the solvent instantly curls the device followed by its swelling and gradual flattening as the top magnet layer (facing down) detaches itself from the rest of the device by stress induced by the swelling. The swelling ratio of the magnetic elastomer is calculated by measuring the change in the lengths of specimens before and after their exposure to the chloroform solvent. Specimens of $2 \times 2.5 \times 6\ mm$ are left in the chloroform solvent for a time period of 24 $hrs$ to ensure their complete swelling as has been done for the measurement of the PDMS swelling ratio (1). After the chloroform wash, the device is transferred to another petri-dish containing solvent chloroform (10 $ml$) which is stirred for another 5 minutes to ensure complete dissolution of the PCTE mold. From the second chloroform wash, the device is further transferred to a third petri-dish containing ethanol solvent. The device retracts back to its original shape and size in a few minutes preparing it for its placement into a pre-prepared PDMS molded chamber attached to a glass slide. The chamber is filled with ethanol and covered with a cover slip to hold the cilia in a fluid environment for a long time while making it easy and safe to handle for observing them under the microscope (Fig. S1,H and I). In a separate configuration the released cilia are placed side-ways in the chamber to view the bending profile of cilia structures under different applied magnetic field conditions (Fig. S1J).

S2. Torque based model for estimating the cilia bending angle

The torque based model predicts the large deformation of the micro/ nano magnetic structures containing magnetic material of susceptibility much higher than 1. The synthesised magnetite particles, having high susceptibility (2), show the characteristic magnetization behaviour without hysteresis or remnant magnetic field (Fig. S3A). When the applied magnetic field is below the saturation limit of the magnetic particles, then the magnetic torque ($\tau_{mag}$) balances the opposing deformation torque ($\tau_{def}$) taking the form (3, 4):

$$\tau_{def} = -\tau_{mag} \quad [1]$$

$$\Rightarrow \frac{\pi E r^4 \theta}{L} = -\frac{\nu |n_r - n_a|}{2\mu_0 n_a n_r} |B|^2 sin(2(\theta - \phi)) \quad [2]$$

The geometric demagnetization factors $n_r$ and $n_a$ along the cilium axis are calculated by taking the long axis of the cilium as the axis of symmetry and are given by (3):

$$n_a = \frac{1}{R^2 - 1}\left(\frac{R}{2\sqrt{R^2-1}} ln\left(\frac{R + \sqrt{R^2-1}}{R - \sqrt{R^2-1}}\right) - 1\right) \quad [3]$$

$$n_r = \frac{1 - n_a}{2} \quad [4]$$

Where $R = L/2r$ is the cilium aspect ratio. The cilium parameters, length $L$ and radius $r$ are known from the PCTE mold thickness and pore radius respectively and are cross checked with the measurements from SEM images of fabricated cilia. For Young's modulus measurement, cubic specimens were prepared by first curing a bulk volume of material in a vacuum oven followed by its sizing into sections of $2 \times 2 \times 2.5\,mm$ size. The bulk material is cured by heating and maintaining it consecutively at a temperatures of 100, 140 and $180^0C$ for a time period of 3, 3 and 2 $hrs$ respectively. Step wise increase in curing is required for removing the gases produced in the material at high temperatures. Specimen sizing is done using a flat edged blade mounted on a micro-precision XYZ linear translational stage assembly, producing specimens of accurate dimensions and right angled edges. The Young's modulus is measured using an in-house built setup measuring the force generated each time the specimen is compressed by a step of $10\,\mu m$. The specimen is compressed to a total of $\sim 25\%$ its length to measure the value of $E$. The magnetic parameters present in the above equation are the applied magnetic field intensity ($B$) and its direction $\phi$ with the vertical axis, (Fig. S3B). These values are computed using a COMSOL model of a $7\,mm$ cube magnet used to measure the bending response of the fabricated cilia. A solid model of the magnet with round chamfered edges ($\sim 100\,\mu m$ radius) is imported from an AutoCAD file to the COMSOL finite element model and the computed values are validated against the values measured along the central vertical axis of the permanent magnet using a magnetic probe from FW Bell. As the cilia bending response is measured by changing in steps the x-distance from 15 to $0\,mm$ while keeping the z-distance fixed, the respective magnetic field intensities $B$ and the directed angles $\phi$ are extracted from the COMSOL model, (Fig. S3C). For each x-position Eq.2 is numerically solved to obtain the only unknown parameter $\theta$ using a Matlab code. Parameter values used in calculating the bending response of all four selected cilia sizes are listed in table S1.

**Table S1.** Computed, calculated and measured parameter and their limits used in Equation 2 for calculating bending angles at different x-positions and plotted in different figures.

| | r ($\mu m$) | L ($\mu m$) | z ($\mu m$) | x ($mm$) | E ($MPa$) | $\phi$ |
|---|---|---|---|---|---|---|
| Fig. 3D | 1.5±0.035 | $47^{+1}_{-0}$ | 600±50 | $0-15$ | 1.2±0.25 | Shown in Fig.S3C |
| Fig. 3E | 0.355±0.005 | $9^{+0.5}_{-0}$ | 500±50 | $0-15$ | 1.2±0.25 | Shown in Fig.S3C |
| Fig. 3,G and H | 1.5±0.035 | $49^{+1}_{-0}$ | 900±50 | $0-12.5$ | 1.2±0.25 | $90^0$ |
| Fig. S4A | 1±0.025 | $23^{+1}_{-0}$ | 600±50 | $0-15$ | 1.2±0.25 | Shown in Fig.S3C |
| Fig. S4,D and E | 1.5 | 49 | 850 | $0-12.5$ | 1.2 | $90^0$ |

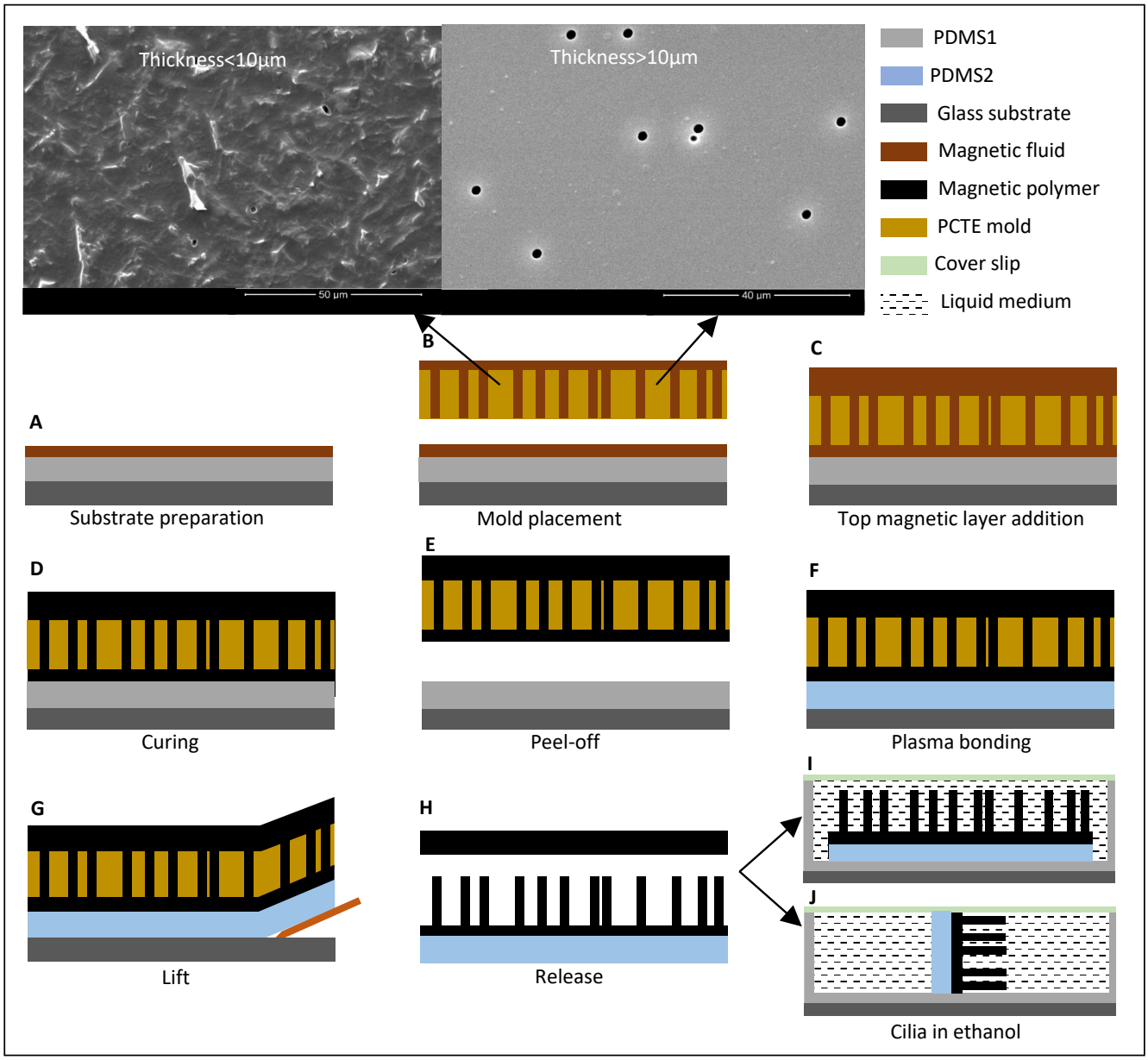


**Fig. S1:** Schematic representation of the molding process: (A) Spin coated PDMS on a glass substrate on top of which magnetic fluid is pasted. (B) PCTE mold with pores filled with magnetic fluid is placed with smooth face on the magnetic fluid layer; arrows point towards the SEM images showing rough and smooth surfaces of molds with thickness less than $10\ \mu m$ and more than $10\ \mu m$ respectively. (C) Top magnetic fluid layer added to mix with the nanofilm and increase its net thickness. (D) Magnetic fluid is cured in an oven to changes to change it into the magnetic polymer. (E-F) The PCTE mold covered with a cured magnetic elastomer is peeled off and plasma-bonded to another PDMS layer. (G) The cilia layer along with the PDMS layer is lifted from the glass substrate before washing. (H) The top layer is detached during washing and the PCTE mold is dissolved in chloroform. (I) The cilia is transferred to a device for top-view visualization. (J) A small section of Cilia device is cut to fit in the $500\ \mu m$-deep chamber for side-view image acquisition.

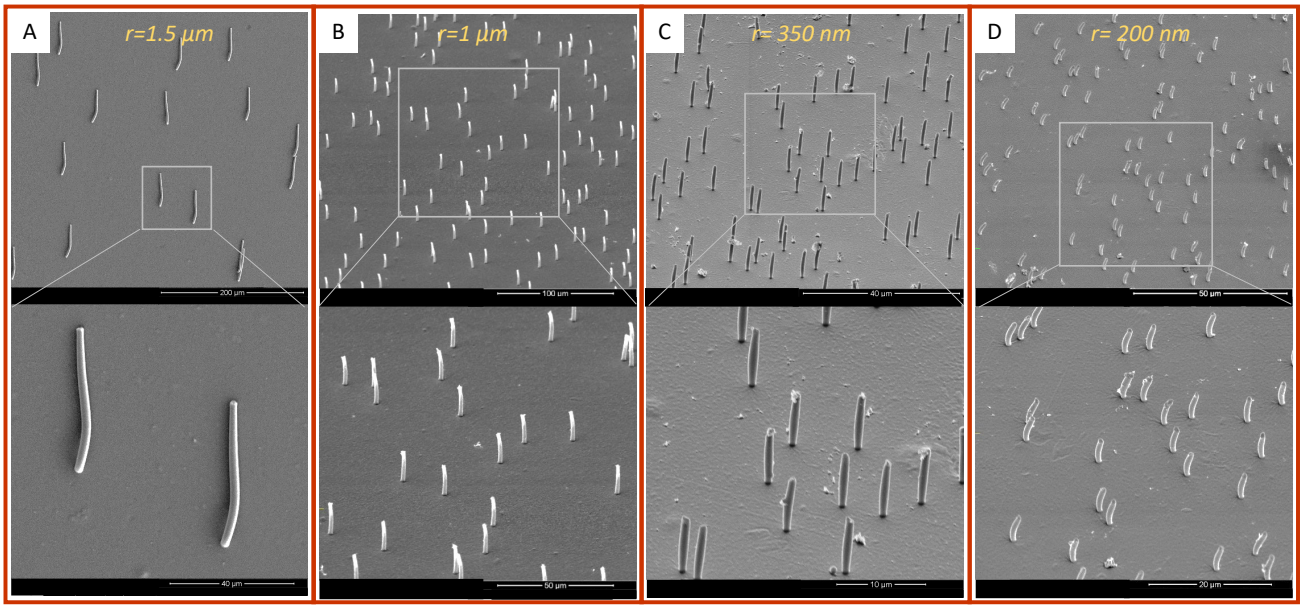


**Fig. S2:** SEM images of micro and nano cilia fabricated and dried using critical-point drying to prevent the cilia collapse when removing the surrounding liquid: (A) Micro cilia with $r = 1.5\ \mu m$, $L = 47\ \mu m$ and density $= 1 \times 10^4\ cm^{-2}$. Images are made at different magnifications. (B) Micro cilia with $r = 1\ \mu m$, $L = 23\ \mu m$ and density $= 1 \times 10^5\ cm^{-2}$. (C) Nano cilia with $r = 350\,nm$, $L = 9\,\mu m$ and density $= 7 \times 10^5\ cm^{-2}$. (D) Nano cilia with $r = 200\,nm$, $L = 6\,\mu m$ and density $= 1 \times 10^6\ cm^{-2}$.

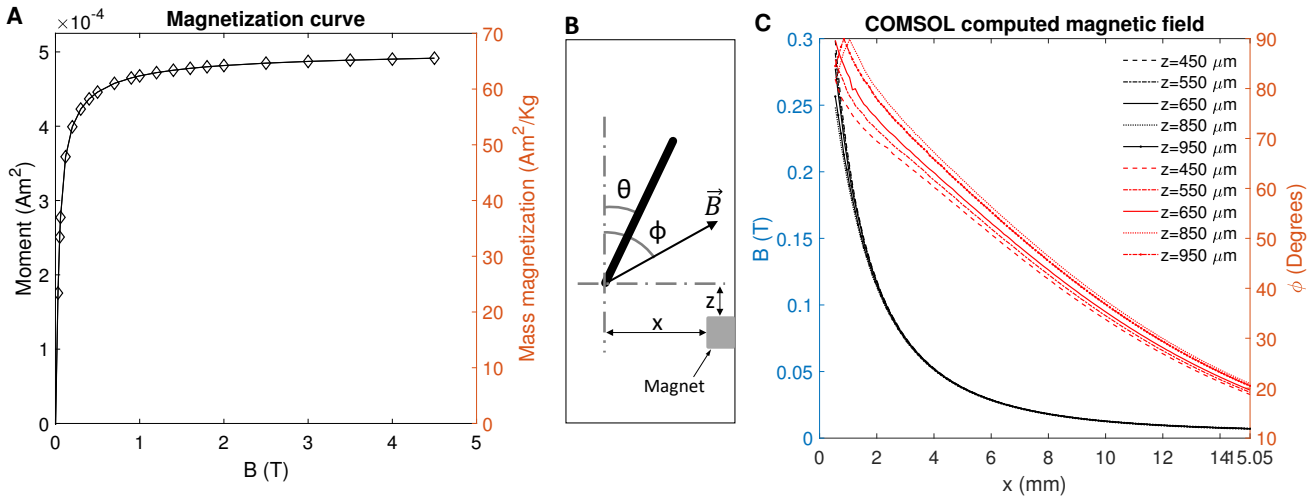


**Fig. S3:** Magnetic particle properties and the external magnetic field intensities: (A) Typical magnetization curve (5, 6) of the synthesized superparamagnetic nano particles $(Fe_3O_2)$ as measured using a bulk quantity of magnetic particles. Sharp increase of the magnetization at the beginning indicates strong response of the particles at lower applied magnetic field intensities. (B) Schematic representation of a cilium and the direction $\phi$ of magnetic field $B$ applied to bend a cilium. (C) Magnetic field intensity $(B)$ and its direction $(\phi)$ as experienced by the cilia applied by an external permanent magnet held at different positions $(x)$ from the cilium under observation. The curves are plotted from the data extracted from a COMSOL model. Three different $z$ values correspond to the distances within which the cilia with micro and nano sizes were positioned while changing the magnet x-position to evaluate the bending response (Table S1).

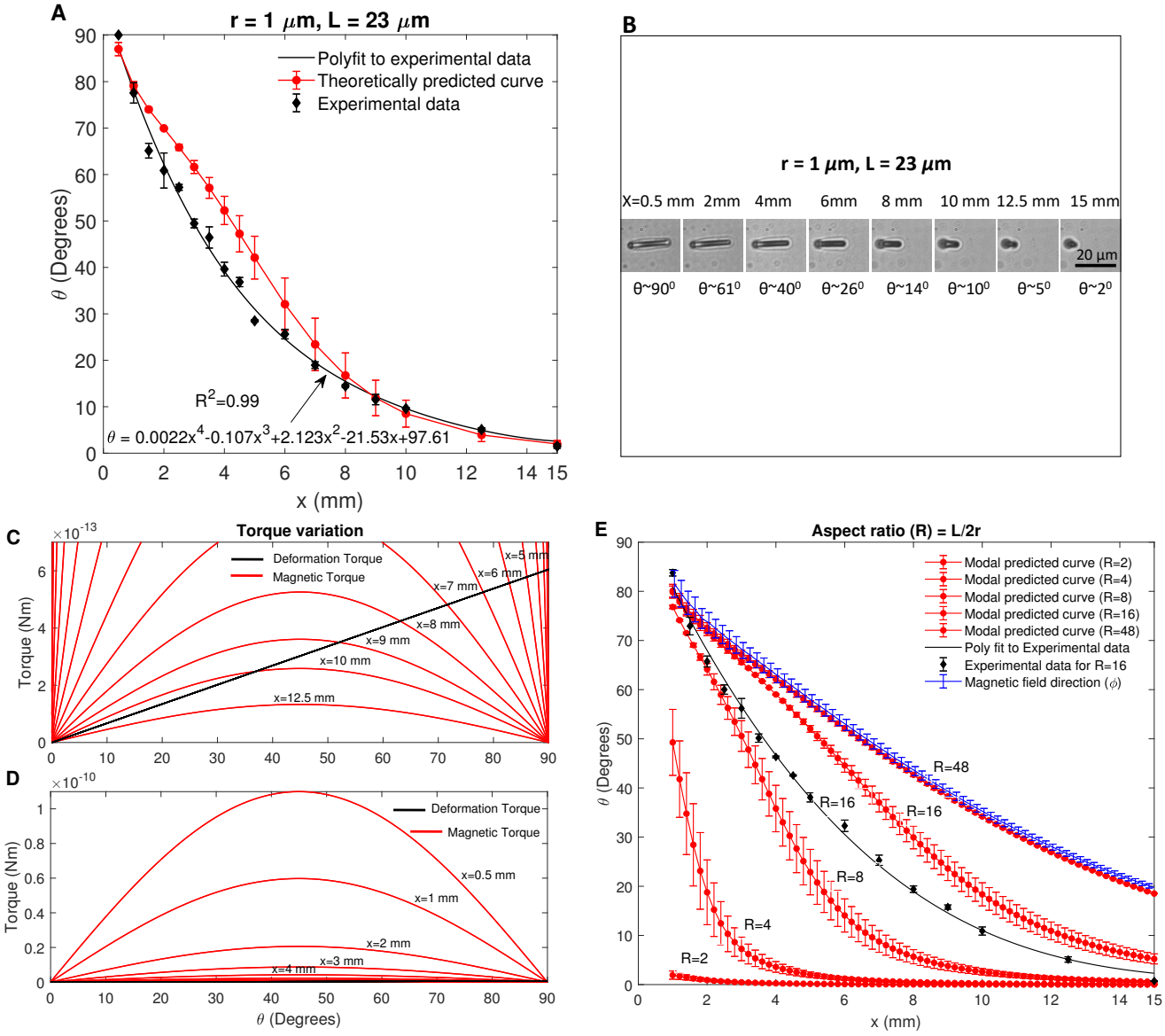


**Fig. S4:** Cilia bending response: (A) Bending behaviour from $0 - 90^0$ of the cilia with nominal radius of $1\ \mu m$ compared with the model results (Movie S6). At large bending angles the maximum difference between the experimental and theoretical data is well within the $30\%$ limit of the model accuracy. Uncertainties of the parameters used in calculating the theoretical values introduce the error bar on the theoretically curve (Table S1). (B) Microscope images (transmission) of a cilium with $r = 1\ \mu m$ and $L = 23\ \mu m$ for various bending angles (top view). (C) Shows the deformation and magnetic torque variation when the cilia bending angles varies form $0$ to $90^0$, while keeping the permanent magnet fixed at different x positions. The actual bending of cilia is taken as the one where deformation and magnetic torque equal each other. Since the deformation torque is much lower than the magnetic torque a magnified plot is shown here with $x$ varying from $5$ to $12.5\ mm$. As the model considers constant radius of curvature for the bent cilia, it predicts lower deformation torque values than the real ones, which results in $30\%$ error compared to the real value. Different parameter values are shown in Table. S1. (D) A zoomed out plot to show the torque variation for x varying from $0.5$ to $4\ mm$. (E) Cilia bending response predicted by the model is plotted against varying $x$ distance for different aspect ratios ($R$, defined as the cilia length over cilia width ratio), varying from $2$ to $48$. At $R = 2$, corresponding to the case of a high bending stiffness cilia, it shows no bending, whereas for high aspect ratio (at $R = 48$ cilia and hence, low bending stiffness cilia), it closely follows the magnetic field direction (blue curve) for all $x$ values. These two cases define two extrema for $R$ for the magnetic material used here for fabricating cilia. Experimental results from cilia with an aspect ratio of $16$ are also shown. These data fall within a $30\%$ range from the predicted values. The parameter values considered here are the same as the one used Fig.3D and given in Table. S1.

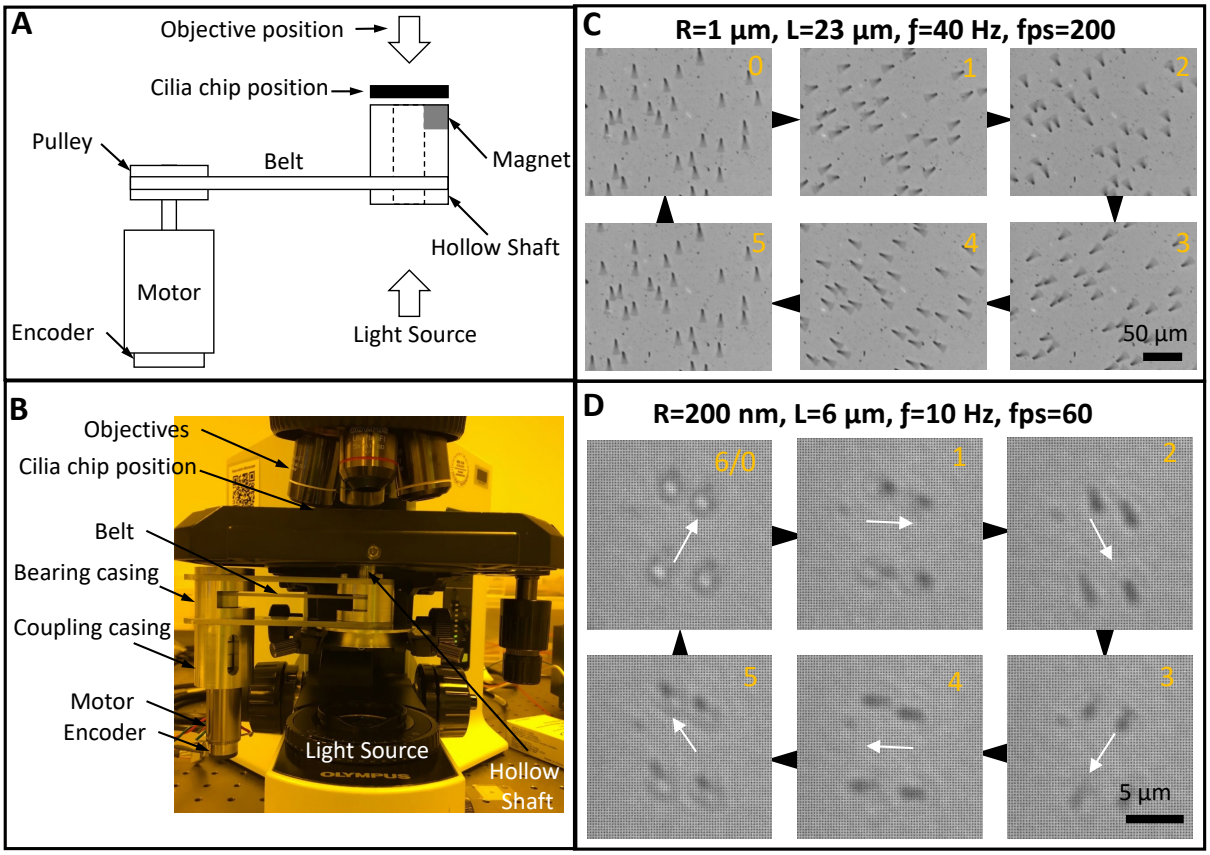


**Fig. S5:** Magnetic actuator setup and motility response of cilia: (A) Schematic representation of the setup used to actuate the cilia by rotating a permanent magnet held on top a hollow shaft to allow light transmission. (B) The setup mounted on a microscope and the position of different parts is indicated. (C) Five frames extracted from a video recorded at $200\ fps$ showing $360^0$ smooth and uninterrupted rotation of micro cilia with $r = 1\ \mu m$ and $L = 23\ \mu m$ rotating at $40\ Hz$ as $200/40 = 5$ frames (frame $5 =$ frame $0$). (D) Nano cilia with $r = 200\ nm$ and $L = 6\ \mu m$ actuated at $10\ Hz$ frequency and recorded at $60$ fps are shown to follow the rotating magnetic field. Arrows indicate the cilia orientation and direction.

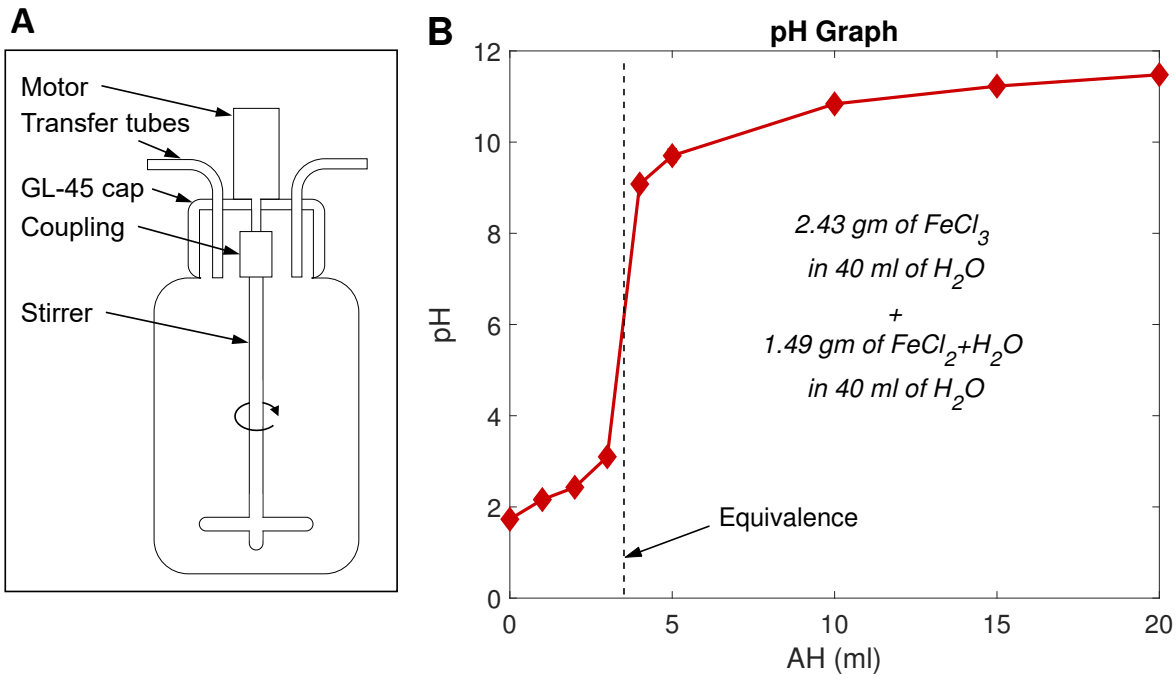


**Fig. S6:** Schematic representation of setup used and the $pH$ plot: (A) The setup and its different parts used for magnetic fluid preparation. (B) The $pH$ is measured in a separate experiment using a $pH$ probe (SB90M5 SympHony from VWR) attached to another modified GL-45 cap holding the probe in the solution while titrating it with ammonium hydroxide solution. The probe is calibrated against three buffer solution with a $pH$ of $3,\ 7$ and $10$ before its use. Multiple experiments show that the error bars in the recorded values are very small indicating strict variation and dependence of the $pH$ with the ammonium hydroxide solution added.

**Movie S1** Bending of micro cilia with $r = 1.5\,\mu m$ and $L = 47\,\mu m$ in steps from a straight vertical position of $0^0$ bending to a maximum of $90^0$ deflection and the corresponding angles as represented in Fig. 3D. Frames in the movie are stacked images captured at increasing bending angles corresponding to different closing-in positions of the actuating magnet mounted on a micro-precision ($10\,\mu m$ least count) linear translational stage. Each image is captured by first adjusting the focus as the bending cilia shifts in its z-position.

**Movie S2** Bending of nano cilia with $r = 350\,nm$ and $L = 9\,\mu m$ from 0 to $90^0$ and the corresponding angles as represented in Fig. 3E. Images captured at different bending angles are stacked after adjusting the focus into a movie.

**Movie S3** Side view of micro cilia with a radius of $1.5\,\mu m$ and a length of $49\,\mu m$ being bent from 0 to $80^0$ and the corresponding angles, as represented in Fig.3H.

**Movie S4** Side view of micro cilia with a radius of $1.5\,\mu m$ and a length of $49\,\mu m$ and actuated by rotating the magnet held at $x = 1.5\,mm$ and $z = 0.9\,mm$ for demonstrating maximum possible bending of cilia.

**Movie S5** Side view of nano cilia with a radius of $350\,nm$ and a length of $9\,\mu m$ being bent by bringing the external permanent closer form $x = 12.5\,mm$ to $x = 0.5\,mm$.

**Movie S6** Bending of micro cilia with $r = 1\,\mu m$ and $L = 23\,\mu m$ from 0 to $90^0$ and the corresponding angles as represented in Fig. S4A.

**Movie S7** Actuation of micro cilia with $r = 1.5\,\mu m$ and $L = 47\,\mu m$ through a full $360^0$ rotation angle at a very large angle of deflection and up to a frequency of $80\,Hz$. Slowed down frames of the video (last few seconds) show cilia with wider tips and narrower bases due to higher linear velocity of tips as compared to the base inducing a linearly decreasing distorted image of the cilia shape from tip to base. The $360^0$ motion of all the four selected micro/ nano cilia is recorded keeping the $x$ and $z$ position of actuating magnet constant at $1.5^{\pm 0.1}\,mm$ and $500^{\pm 50}\,\mu m$ respectively.

**Movie S8** Actuation of micro cilia with $r = 1\,\mu m$ and $L = 23\,\mu m$ through $360^0$ rotating angle and up to a frequency of $80\,Hz$.

**Movie S9** Actuation of nano cilia with $r = 350\,nm$ and $L = 9\,\mu m$ through $360^0$ rotation and up to a frequency of $10\,Hz$. No appreciable visual change is observed at frequencies higher than $10\,Hz$. Recordings done at higher fps where used

to confirm that even at higher frequencies the cilia motion continued to follow the magnetic field direction.

**Movie S10** Actuation of nano cilia with $r = 200\,nm$ and $L = 6\,\mu m$ through $360^0$ rotation and up to a frequency of $10\,Hz$. Given the diameter of cilia, equivalent to the lower limit of visible light wavelength, combined with the effects of back illuminating light travelling through air to liquid to air medium, and recordings done at higher magnifications having smaller focal depth, only a blurred shape of the nano cilia is possible to capture.

**Movie S11** Comparison of artificial cilia system fabricated with radius, length, distribution and frequency of rotation equivalent to the cilia found on the Medakafish embryo. Cilia formed in the embryonic nodes during the embryonic growth of most of the mammal species perform a tilted conical motion (TCM) producing flow in one direction (7). The artificial cilia system shown here performing a $360^0$ rotatory motion instead of TCM, however a TCM can be easily achieved by shifting the centre of rotation of the magnet with respect to the cilia.

**Movie S12** Cilia are actuated at different frequencies in water medium after transferring them from ethanol by first rinsing them in a solution containing soap or Triton X-100 to change the cilia surface from a hydrophobic to hydrophilic nature.

## 1. References


1. Jessamine Ng Lee, Cheolmin Park, and George M Whitesides. Solvent compatibility of poly (dimethylsiloxane)-based microfluidic devices. *Analytical chemistry*, 75(23):6544–6554, 2003.
2. John F Schenck. The role of magnetic susceptibility in magnetic resonance imaging: Mri magnetic compatibility of the first and second kinds. *Medical physics*, 23(6):815–850, 1996.
3. Jake J Abbott, Olgaç Ergeneman, Michael P Kummer, Ann M Hirt, and Bradley J Nelson. Modeling magnetic torque and force for controlled manipulation of soft-magnetic bodies. *IEEE Transactions on Robotics*, 23(6):1247–1252, 2007.
4. Robert M Judith, Jay K Fisher, Richard Chasen Spero, Briana L Fiser, Adam Turner, Bruce Oberhardt, RM Taylor, Michael R Falvo, and Richard Superfine. Micro-elastometry on whole blood clots using actuated surface-attached posts (asaps). *Lab on a Chip*, 15(5):1385–1393, 2015.
5. M Kryszewski and JK Jeszka. Nanostructured conducting polymer composites—superparamagnetic particles in conducting polymers. *Synthetic Metals*, 94(1):99–104, 1998.
6. Benjamin A Evans, Briana L Fiser, Willem J Prins, Daniel J Rapp, Adam R Shields, Daniel R Glass, and R Superfine. A highly tunable silicone-based magnetic elastomer with nanoscale homogeneity. *Journal of magnetism and magnetic materials*, 324(4):501–507, 2012.
7. Yasushi Okada, Sen Takeda, Yosuke Tanaka, Juan-Carlos Izpisúa Belmonte, and Nobutaka Hirokawa. Mechanism of nodal flow: a conserved symmetry breaking event in left-right axis determination. *Cell*, 121(4):633–644, 2005.